

Supplementary Information

A natural food-grade supramolecular self-assembly system for creation of hierarchically structured hydrogels

Xinke Yu,^{a,d} Jiyang Cai,^{a,d} Mengyue Xu,^{a,b} Qing Li,^a Yunyi Yang,^a Zhili Wan^{a,c,*} and Xiaoquan

Yang^a

^a Laboratory of Food Proteins and Colloids, School of Food Science and Engineering, Guangdong Province Key Laboratory for Green Processing of Natural Products and Product Safety, South China University of Technology, Guangzhou 510640, China

^b Laboratory of Physics and Physical Chemistry of Foods, Wageningen University, Bornse Weilanden 9, 6708WG Wageningen, The Netherlands

^c Overseas Expertise Introduction Center for Discipline Innovation of Food Nutrition and Human Health (111 Center), Guangzhou 510640, China

^d These authors contributed equally: Xinke Yu, Jiyang Cai.

Submitted to: *Nanoscale*

*Corresponding author: Zhili Wan

E-mail: zhiliwan@scut.edu.cn, Fax: (086) 20-87114263

Experimental details

Chemicals

Glycyrrhizic acid mono ammonium salt (GA, purity >98%) was purchased from Thermo Fisher (USA). κ -carrageenan (CG), guar gum (GG), and xanthan gum (XG) were purchased from Shanghai Aladdin Co., Ltd. (China). Sodium chloride (NaCl) and potassium chloride (KCl) were bought from Chemical Reagent Co., Ltd. (China). Milli-Q water (18.2 M Ω cm) was used, and all chemicals used were of analytical grade.

Preparation of GA-CG hydrogels

Stock solutions of GA (8 wt%) and CG (2 wt%) were prepared by dissolving GA and CG powder in water and heating at 80 °C under mild agitation to obtain a transparent solution. NaCl and KCl (2M) were prepared by dissolving salts in water and adjusting the pH to 4.0. Then, GA solution, CG solution, and salt solution were completely mixed at different volume ratios under the heating condition (80 °C) to acquire the desired sample concentration. The resultant samples were stored overnight (12 h) at room temperature (25 °C) before further use. The final concentration of GA and CG is 2 wt% and 1 wt% respectively, and the salt concentration ranges from 0-500 mM. The corresponding hydrogel samples are termed GA, CG, GA-CG, GA-CG-Na_x, and GA-CG-K_x, respectively (x represents the salt concentration). The gelation of the sample was determined by the tube inverted test, and the gel formation was verified if no visual fluidity was observed after 1 min of tube inversion. For GG and XG, the hydrogels were prepared in the same process as described above.

Cryo scanning electron microscopy (Cryo-SEM)

The hydrogel samples were fixed on a holder and snap-frozen with liquid nitrogen slush before

being transferred into a cryo chamber (PP3010T, Quorum, UK) at -140 °C. The samples were afterward sublimated for 30 min at -90 °C to remove frost artifacts. Finally, the samples were scanned with a scanning electron microscope (S-4800, Hitachi) at 3 kV.

Field emission scanning electron microscopy (FE-SEM)

The microstructures of freeze-dried hydrogel samples were observed on a Zeiss Merlin field emission scanning electron microscope (Zeiss, Germany). The samples were carefully transferred and firmly attached to a holder, and then sputter-coated with gold (JEOL JFC-1200 fine coater, Japan) before imaging at 5 kV.

Atomic force microscopy (AFM)

A droplet of hydrogel sample was deposited on freshly cleaved mica and dried on air. AFM measurements were performed by using a Bruker Dimension Icon atomic force microscopy (Bruker, Germany) in tapping mode. The AFM images were analyzed using NanoScope Analysis software.

X-ray Diffraction (XRD)

XRD measurements were carried out by an X-ray diffractometer (X'pert Powder, PANalytical) in symmetric reflection mode. Freeze-dried hydrogel samples were scanned from 2 to 60° at a scanning rate of 15° min⁻¹.

Fourier transform infrared spectroscopy (FTIR)

The FTIR spectra of freeze-dried hydrogel samples were recorded at 400–4000 cm⁻¹ using an FTIR spectrophotometer (Thermo Fisher, USA) equipped with a narrow-band mercury cadmium telluride detector with a resolution of 2 cm⁻¹.

X-ray photoelectron spectroscopy (XPS)

XPS measurements were performed using a Kratos Axis Supra⁺ XPS instrument (Kratos, UK). Al K α radiation was used, and the chamber pressure was less than 5×10^{-9} torr during operation. The XPS spectra were scanned with the pass energy of 160 eV and 40 eV for full and narrow spectra, respectively. Thermo Scientific Avantage software was used for data analysis. The data was calibrated based on the C 1s peak at 284.8 eV, and a smart-type background was used.

Small Angle X-ray Scattering (SAXS)

SAXS measurements were conducted on a SAXS instrument (Xeuss 2.0, Xenocs, France). The X-ray source was MetalJet-D2 (Dectris Ltd.) with a wavelength of $\lambda = 0.134144$ nm and the sample-to-detector distance was about 2.5 m. The chamber containing hydrogel samples was placed on the optical path of the SAXS device. The X-ray beam entered through the Kapton window at an angle perpendicular to the hydrogel sample surface and 2D SAXS data were collected using a Pilatus3R 1 M detector with a pixel size of 0.172×0.172 mm². The 2D data were integrated into the one-dimensional scattering function $I(q)$ as a function of the magnitude of the scattering vector

$$q = \frac{4\pi}{\lambda} \sin\left(\frac{\theta}{2}\right) \quad \#(1)$$

where θ is the scattering angle.

The data are subtracted by the background intensity. The data was analyzed by BioXTAS RAW.^{1,2} The pair distance distribution function $P(r)$ is determined by GNOM software in the ATSAS package,³ of which BioXTAS RAW provides an interface.

Zeta potential measurements

The Zeta potential of hydrogel samples was measured using a Zetasizer Nano ZS (Malvern, UK).

The measurements were carried out at 25 °C in triplicate.

Rheological measurements

The rheological properties of hydrogel samples were investigated using a Haake MARS60 rheometer (Haake, Germany), and a parallel plate geometry (35 mm diameter, 1 mm gap) was used. All measurements were carried out at 25 °C and samples were allowed to relax for 2 min before rheological tests.

Small amplitude oscillation shear (SAOS) measurements

Frequency sweep tests were conducted with the angular frequency range from 0.1 to 100 rad/s, while the strain was kept constant at 0.1% in the linear viscoelastic region (LVR).

Large amplitude oscillation shear (LAOS) measurements

LAOS measurements were performed with strain sweep tests, which were measured over the strain range of 0.01-1000% at a fixed angular frequency of 6.28 rad/s. The yield strain is defined here as the value of the strain amplitude at which the storage modulus (G') deviates by more than 5% from its strain-independent value within the LVR,^{4,5} and correspondingly, the yield stress is the stress observed at the yield strain. Additionally, the flow strain and stress are defined as the strain and stress values at the crossover point, where the G' equals the G'' .⁶ Based on these definitions, the rheological behaviors of hydrogels can be quantified and accurately characterized.

To analyze the nonlinear responses of hydrogels, the torque-deformation waveform data was collected at different strains (1, 5, 11, 49, 98, and 500%) with a constant angular frequency (6.28

rad/s). According to the method of McKinley and co-workers,⁷ based on a Chebyshev polynomial based stress decomposition, the torque-deformation waveform data can be further analyzed using the MITLaos software (Version 2.2 beta), to construct Lissajous-Bowditch plots and determine the Chebyshev coefficients. The intracycle strain stiffening ratio (S factor) and intracycle shear thickening ratio (T factor), as defined in Eqs (2) and (3), were determined.

$$S = \frac{G'_L - G'_M}{G'_L} \#(2)$$

$$T = \frac{\eta'_L - \eta'_M}{\eta'_L} \#(3)$$

In equation (2), G'_L is the large-strain modulus or secant modulus evaluated at the maximum imposed strain, and G'_M is the minimum-strain modulus or tangent modulus at $\gamma=0$. In equation (3), η'_L is the large-rate dynamic viscosity, and η'_M is the minimum-rate dynamic viscosity.⁷

Compression test

The compression test of hydrogel samples was performed using a universal testing machine (Instron 5943, USA). A cylindrical probe of 25 mm was used to compress hydrogels in cylinder shape to a depth of 60% of their original height at a rate of 0.2 mm/s with a 0.1 g trigger value. Fracture strain and fracture stress are calculated based on the stress-strain curves.

In vitro controlled cargo release

To investigate the bioactive release behaviors of hydrogels under different pH conditions, we selected VB₁₂ as a model hydrophilic cargo to prepare functional hydrogels. Appropriate amounts of VB₁₂-loaded (1 mg/mL) hydrogels were weighed into beakers, followed by adding HCl-NaH₂PO₄

solution (0.2 M) with pH 2.5 or PBS solutions (0.2M) with pH 7.5 and then incubating under mild stirring (100 rpm) at 37 °C. At predetermined time intervals, the released solution was taken out, and the absorbance of the released VB₁₂ was measured at 361 nm using a UV–vis spectrophotometer (C40 Touch, Implen, Germany). Subsequently, the solution after testing was returned to the beakers to maintain the constant volume. VB₁₂ concentration was calculated according to the calibration equation. The calibration equations were found to be $A = 0.0163C - 0.0005$ ($R^2 = 0.9996$) at pH 2.5 and $A = 0.0149C + 0.0016$ ($R^2 = 0.9992$) at pH 7.5. The release ratio of VB₁₂ was calculated according to the equation below:

$$\text{Release ratio (\%)} = \frac{C_t}{C_0} \times 100 \#(4)$$

where C_0 and C_t mean the initial VB₁₂ concentration and released VB₁₂ concentration at time t , respectively.

To understand the release mechanism of VB₁₂ in hydrogels, the release data were analyzed to describe the release mechanism and could be fitted to Eqs (1) zero order, (2) first order, (3) Higuchi,⁸ and (4) Ritger-Peppas models.⁹

$$M_t/M_\infty = at \#(5)$$

$$\ln(1 - M_t/M_\infty) = -at \#(6)$$

$$M_t/M_\infty = at^{1/2} \#(7)$$

$$M_t/M_\infty = bt^a \#(8)$$

where M_t and M_∞ correspond to the cumulative amount of drug released at time t and equilibrium, respectively. a is the release exponent, and b is the release rate constant. These models represent the

different diffusion patterns of cargo as a function of time.

Stability measurements

Light stability

For the light stability measurements, VB₁₂-loaded GA-CG hydrogels were incubated under the light irradiation (12 W) in a sealed lighting device for 4 h. The light stability of free VB₁₂ in the pure water as a control was also tested under the same test condition. The residual amount of VB₁₂ was analyzed by recording the absorbance at 361 nm, and the retention ratio of VB₁₂ were calculated according to the following equation:

$$\text{Retention ratio (\%)} = \frac{C_1}{C_0} \times 100 \#(9)$$

where C_0 and C_1 mean the initial VB₁₂ concentration and VB₁₂ concentration after test, respectively.

Thermal stability

For the thermal stability measurements, VB₁₂-loaded GA-CG hydrogels were placed into a sealed vial, and then incubated in a water-bath at 80 °C for 4 h. The thermal stability of free VB₁₂ in the pure water as a control was also tested under the same test condition. The residual amount of VB₁₂ was analyzed by recording the absorbance at 361 nm, and the retention ratio of VB₁₂ were calculated according to the equation (9).

Statistical analysis

All testing was performed in triplicate unless specifically mentioned and results were presented as mean \pm standard deviation for all measurements. One-way Analysis of variance (ANOVA) of the

data was performed using the OriginPro 2021 software. LSD's test was used for the comparison of mean values among samples using a level of significance of 5%.

Reference for supplementary information

1 J. B. Hopkins, R. E. Gillilan and S. Skou, *J. Appl. Cryst.*, 2017, **50**, 1545–1553.

2 J. B. Hopkins, *J. Appl. Cryst.*, 2024, **57**, 194–208.

3 D. I. Svergun, *J. Appl. Cryst.*, 1992, **25**, 495–503.

4 W.-H. Shih, W. Y. Shih, S.-I. Kim, J. Liu and I. A. Aksay, *Phys. Rev. A*, 1990, **42**, 4772–4779.

5 N. M. Wereley, A. Chaudhuri, J.-H. Yoo, S. John, S. Kotha, A. Suggs, R. Radhakrishnan, B. J. Love and T. S. Sudarshan, *J. Intell. Mater. Syst. Struct.*, 2006, **17**, 393–401.

6 F. K. G. Schreuders, L. M. C. Sagis, I. Bodnár, R. M. Boom and A. J. van der Goot, *Sci. Rep.*, 2022, **12**, 1334.

7 R. H. Ewoldt, A. E. Hosoi and G. H. McKinley, *J. Rheol.*, 2008, **52**, 1427–1458.

8 D. R. Paul, *Int. J. Pharm.*, 2011, **418**, 13–17.

9 R. Huang, W. Qi, L. Feng, R. Su and Z. He, *Soft Matter*, 2011, **7**, 6222.

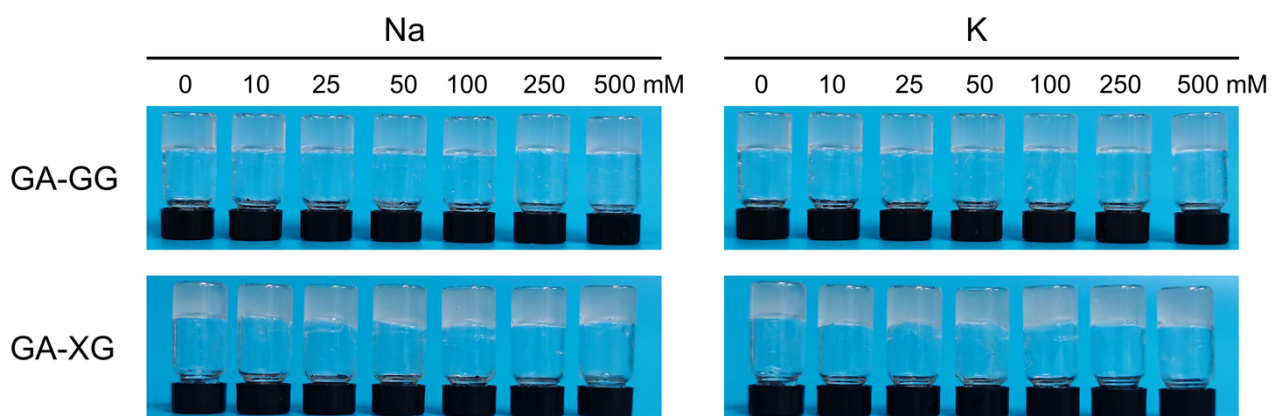


Fig. S1. Digital photos for the gelation experiments of the GA-GG and GA-XG with Na⁺ and K⁺.

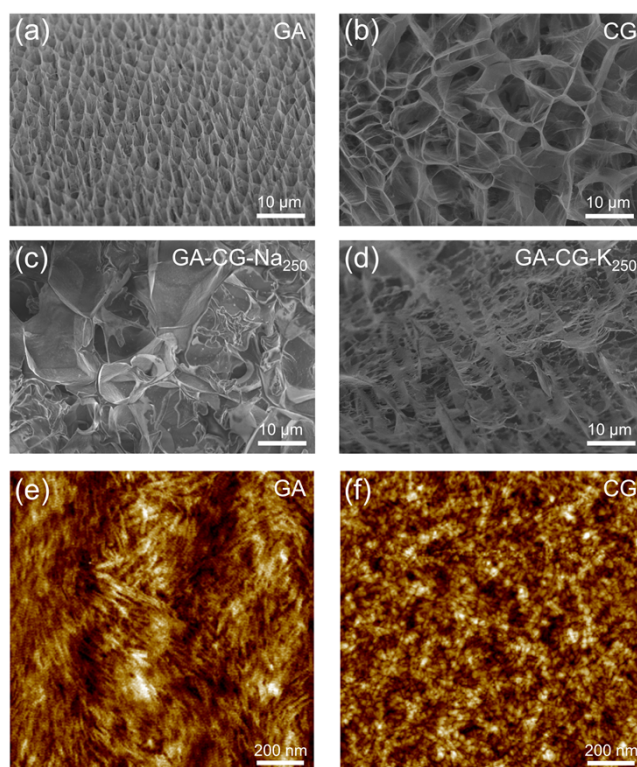


Fig. S2. Cryo-SEM images of GA (a), CG (b), GA-CG-Na₂₅₀ (c), and GA-CG-K₂₅₀ (d). AFM height images of GA (e) and CG (f).

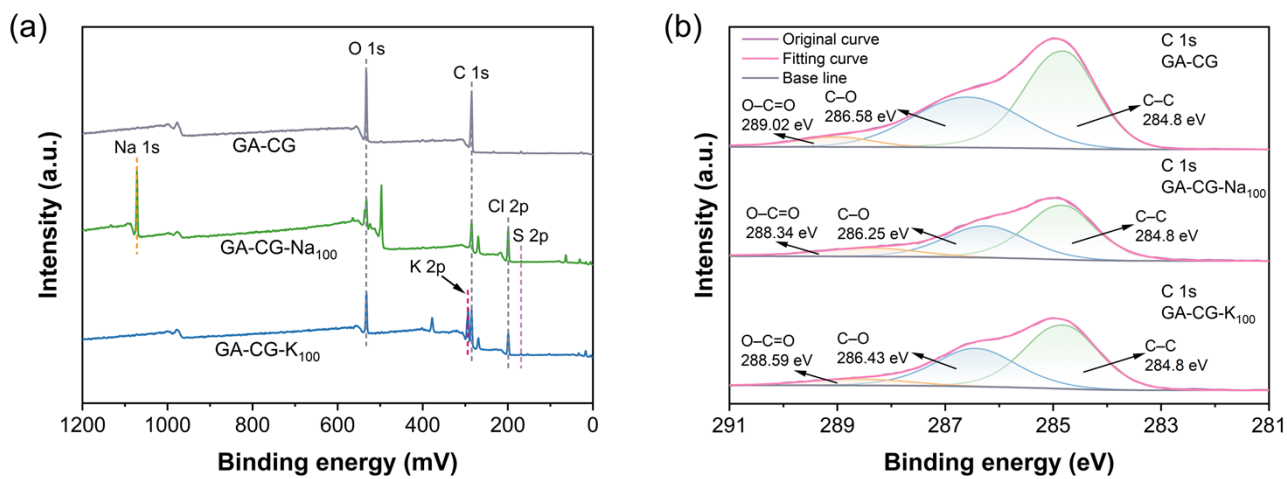


Fig. S3. XPS survey spectra (a) and high-resolution XPS C 1s spectra (b) of GA-CG hydrogels.

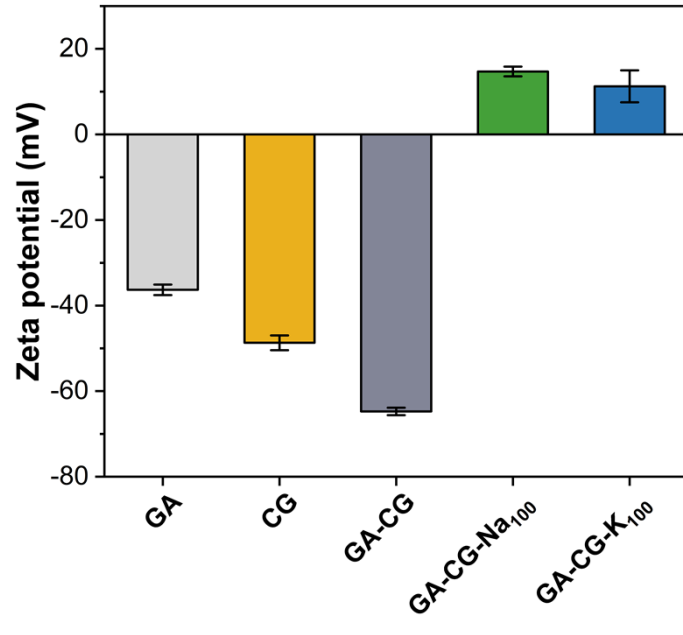


Fig. S4. Zeta potential of GA-CG hydrogels.

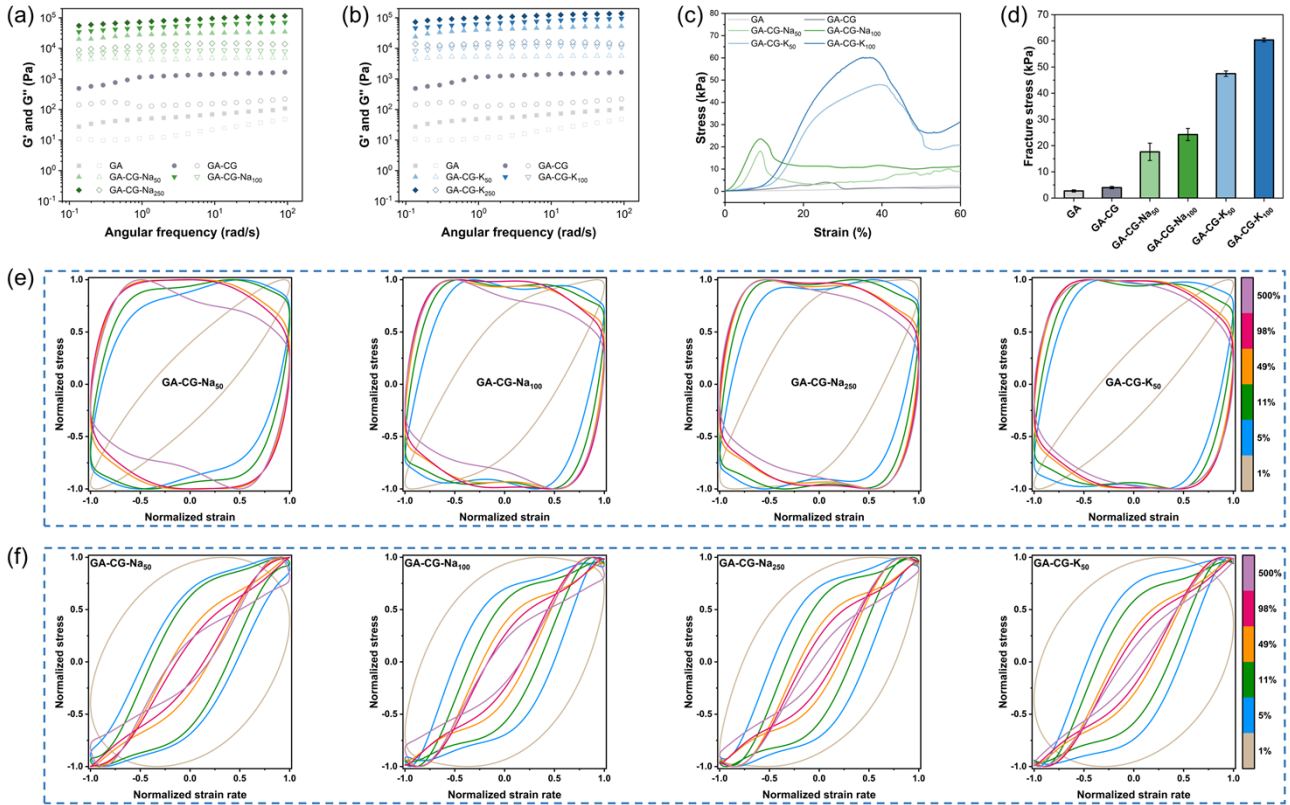


Fig. S5. Frequency sweeps of GA-CG-Na_x (a) and GA-CG-K_x (b) samples. Compression stress-strain profiles (c) and fracture stress (d) of hydrogel samples. Elastic (e) and viscous (f) Lissajous-Bowditch loops of hydrogel samples, acquired at the frequency of 6.28 rad/s and different strains of 1, 5, 11, 49, 98, and 500%. Stress, strain, and strain rate data are normalized with respect to their corresponding maximum values in the oscillation cycle.

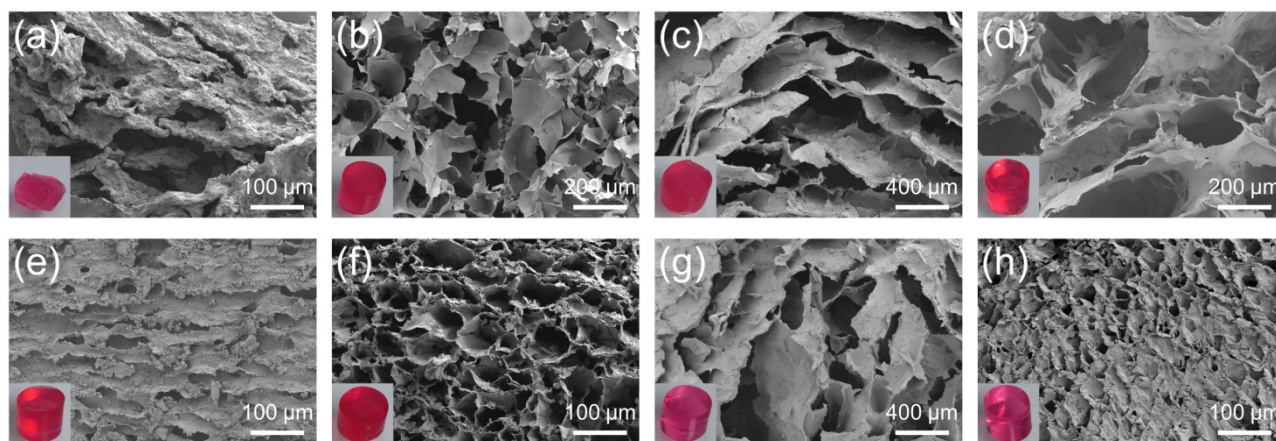


Fig. S6. FE-SEM images of GA (a), GA-CG (b), GA-CG-Na₅₀ (c), GA-CG-Na₁₀₀ (d), GA-CG-K₅₀ (e), and GA-CG-K₁₀₀ (f) after 24 h in simulated gastric fluid at pH 2.5. FE-SEM images of GA-CG-K₅₀ (g) and GA-CG-K₁₀₀ (h) after 24 h in simulated intestinal fluid at pH 7.5.

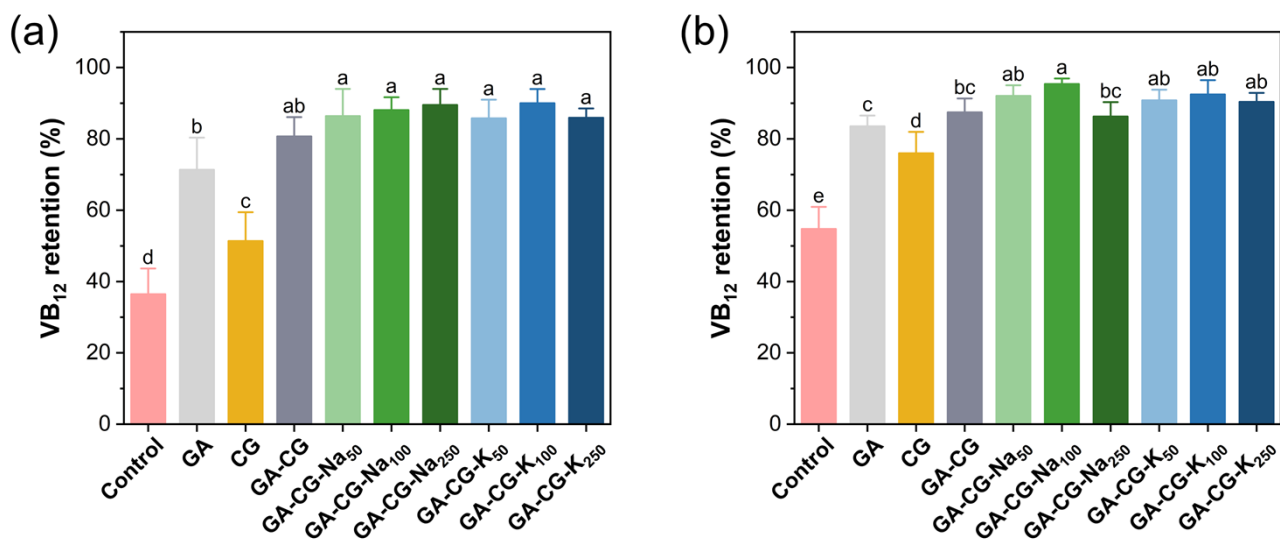


Fig. S7. Retention of VB₁₂ in the GA-CG hydrogels after light (a) and thermal (b) treatments.

Different letters in each column indicate significant differences between groups ($p < 0.05$).

Table S1. Viscoelastic parameters at the critical point and flow point of hydrogel samples.

Samples	G'_{LVR} (Pa)	Yield strain (%)	Yield stress (Pa)	Flow strain (%)	Flow stress (Pa)
GA	55.15 ± 0.01^g	2.15 ± 0.21^a	1.06 ± 0.04^f	58.94 ± 1.82^a	10.49 ± 0.34^e
GA-CG	1096.5 ± 37.5^g	1.30 ± 0.18^b	13.47 ± 1.90^f	8.17 ± 0.01^c	39.39 ± 0.95^e
GA-CG-Na ₅₀	29980 ± 1047^f	0.43 ± 0.01^c	127.15 ± 3.61^e	2.10 ± 0.09^{dc}	134.35 ± 0.49^d
GA-CG-Na ₁₀₀	51043 ± 2224^d	0.34 ± 0.02^d	166.45 ± 0.21^d	1.52 ± 0.18^{dc}	215.8 ± 19.1^c
GA-CG-Na ₂₅₀	91234 ± 984^b	0.30 ± 0.05^d	276.55 ± 5.87^c	0.79 ± 0.08^e	339.7 ± 10.6^a
GA-CG-K ₅₀	33567 ± 1679^e	0.59 ± 0.07^c	170.15 ± 0.07^d	2.40 ± 0.48^d	200.4 ± 21.3^c
GA-CG-K ₁₀₀	59518 ± 1764^c	0.49 ± 0.06^c	298.21 ± 4.95^b	1.32 ± 0.15^{dc}	276.8 ± 24.5^b
GA-CG-K ₂₅₀	97475 ± 1761^a	0.43 ± 0.02^c	374.5 ± 18.5^a	1.37 ± 0.32^{dc}	362.1 ± 12.7^a

Results are presented as mean \pm standard deviation. Different letters in each column indicate significant differences between groups ($p < 0.05$).

Table S2. VB₁₂ release kinetic model fitting in simulated gastric fluid at pH 2.5. The equations implemented in OriginPro 2021, the Value of R^2 , and coefficient obtained after the fitting of models.

Samples	Release kinetics model	Equation	R^2	Coefficient
GA	Zero order model	$M_t/M_\infty = at$	0.86001	$a = 0.06133$
	First order model	$\ln(1 - M_t/M_\infty) = -at$	0.98678	$a = 0.16592$
	Higuchi model	$M_t/M_\infty = at^{1/2}$	0.98412	$a = 0.24501$
	Ritger-Peppas model	$M_t/M_\infty = bt^a$	0.99387	$b = 0.34688$ $a = 0.38159$
CG	Zero order model	$M_t/M_\infty = at$	0.76555	$a = 0.47641$
	First order model	$\ln(1 - M_t/M_\infty) = -at$	0.95888	$a = 1.36671$
	Higuchi model	$M_t/M_\infty = at^{1/2}$	0.87251	$a = 0.6115$
	Ritger-Peppas model	$M_t/M_\infty = bt^a$	0.80307	$b = 0.71988$ $a = 0.34923$
GA-CG	Zero order model	$M_t/M_\infty = at$	0.78565	$a = 0.05681$
	First order model	$\ln(1 - M_t/M_\infty) = -at$	0.97252	$a = 0.17084$
	Higuchi model	$M_t/M_\infty = at^{1/2}$	0.94565	$a = 0.23278$
	Ritger-Peppas model	$M_t/M_\infty = bt^a$	0.99513	$b = 0.29776$ $a = 0.42849$
GA-CG-Na ₅₀	Zero order model	$M_t/M_\infty = at$	0.80129	$a = 0.06256$
	First order model	$\ln(1 - M_t/M_\infty) = -at$	0.87781	$a = 0.30836$
	Higuchi model	$M_t/M_\infty = at^{1/2}$	0.95247	$a = 0.25473$
	Ritger-Peppas model	$M_t/M_\infty = bt^a$	0.99327	$b = 0.45346$ $a = 0.30844$

GA-CG-Na ₁₀₀	Zero order model	$M_t/M_\infty = at$	0.82721	$a = 0.05711$
	First order model	$\ln(1 - M_t/M_\infty) = -at$	0.97286	$a = 0.15567$
	Higuchi model	$M_t/M_\infty = at^{1/2}$	0.96169	$a = 0.22996$
	Ritger-Peppas model	$M_t/M_\infty = bt^a$	0.99533	$b = 0.38005$ $a = 0.33246$
GA-CG-Na ₂₅₀	Zero order model	$M_t/M_\infty = at$	0.82501	$a = 0.05724$
	First order model	$\ln(1 - M_t/M_\infty) = -at$	0.97273	$a = 0.13843$
	Higuchi model	$M_t/M_\infty = at^{1/2}$	0.97627	$a = 0.23255$
	Ritger-Peppas model	$M_t/M_\infty = bt^a$	0.99855	$b = 0.35015$ $a = 0.35953$
GA-CG-K ₅₀	Zero order model	$M_t/M_\infty = at$	0.84054	$a = 0.06018$
	First order model	$\ln(1 - M_t/M_\infty) = -at$	0.98479	$a = 0.16611$
	Higuchi model	$M_t/M_\infty = at^{1/2}$	0.97812	$a = 0.24244$
	Ritger-Peppas model	$M_t/M_\infty = bt^a$	0.99577	$b = 0.36692$ $a = 0.35945$
GA-CG-K ₁₀₀	Zero order model	$M_t/M_\infty = at$	0.85498	$a = 0.06455$
	First order model	$\ln(1 - M_t/M_\infty) = -at$	0.98694	$a = 0.18561$
	Higuchi model	$M_t/M_\infty = at^{1/2}$	0.98682	$a = 0.259$
	Ritger-Peppas model	$M_t/M_\infty = bt^a$	0.99666	$b = 0.34452$ $a = 0.39974$
GA-CG-K ₂₅₀	Zero order model	$M_t/M_\infty = at$	0.79049	$a = 0.0556$
	First order model	$\ln(1 - M_t/M_\infty) = -at$	0.9609	$a = 0.13958$
	Higuchi model	$M_t/M_\infty = at^{1/2}$	0.9599	$a = 0.22883$
	Ritger-Peppas	$M_t/M_\infty = bt^a$	0.99758	$b = 0.38519$

model

$a = 0.32427$

Table S3. VB₁₂ release kinetic model fitting in simulated intestinal fluid at pH 7.5. The equations implemented in OriginPro 2021, the Value of R^2 , and coefficient obtained after the fitting of models.

Samples	Release kinetics model	Equation	R^2	Coefficient
GA	Zero order model	$M_t/M_\infty = at$	0.75757	$a = 0.99$
	First order model	$\ln(1 - M_t/M_\infty) = -at$	0.85995	$a = 4.60517$
	Higuchi model	$M_t/M_\infty = at^{1/2}$	0.92359	$a = 1.06313$
	Ritger-Peppas model	$M_t/M_\infty = bt^a$	0.64478	$b = 0.99045$ $a = 0.0056$
CG	Zero order model	$M_t/M_\infty = at$	0.71895	$a = 0.47641$
	First order model	$\ln(1 - M_t/M_\infty) = -at$	0.95041	$a = 1.61357$
	Higuchi model	$M_t/M_\infty = at^{1/2}$	0.89251	$a = 0.69794$
	Ritger-Peppas model	$M_t/M_\infty = bt^a$	0.75764	$b = 0.65358$ $a = 0.59772$
GA-CG	Zero order model	$M_t/M_\infty = at$	0.85945	$a = 0.23207$
	First order model	$\ln(1 - M_t/M_\infty) = -at$	0.84335	$a = 1.53506$
	Higuchi model	$M_t/M_\infty = at^{1/2}$	0.98504	$a = 0.52438$
	Ritger-Peppas model	$M_t/M_\infty = bt^a$	0.96609	$b = 0.54047$ $a = 0.4746$
GA-CG-Na ₅₀	Zero order model	$M_t/M_\infty = at$	0.92981	$a = 0.24393$
	First order model	$\ln(1 - M_t/M_\infty) = -at$	0.83085	$a = 1.56034$
	Higuchi model	$M_t/M_\infty = at^{1/2}$	0.98134	$a = 0.52891$
	Ritger-Peppas model	$M_t/M_\infty = bt^a$	0.97734	$b = 0.45398$ $a = 0.60158$

GA-CG-Na ₁₀₀	Zero order model	$M_t/M_\infty = at$	0.93179	$a = 0.3075$
	First order model	$\ln(1 - M_t/M_\infty) = -at$	0.75569	$a = 2.06953$
	Higuchi model	$M_t/M_\infty = at^{1/2}$	0.97979	$a = 0.56102$
	Ritger-Peppas model	$M_t/M_\infty = bt^a$	0.96076	$b = 0.51932$ $a = 0.57965$
GA-CG-Na ₂₅₀	Zero order model	$M_t/M_\infty = at$	0.56648	$a = 0.20582$
	First order model	$\ln(1 - M_t/M_\infty) = -at$	0.9782	$a = 1.72133$
	Higuchi model	$M_t/M_\infty = at^{1/2}$	0.82656	$a = 0.52474$
	Ritger-Peppas model	$M_t/M_\infty = bt^a$	0.65864	$b = 0.76665$ $a = 0.25558$
GA-CG-K ₅₀	Zero order model	$M_t/M_\infty = at$	0.81651	$a = 0.09836$
	First order model	$\ln(1 - M_t/M_\infty) = -at$	0.85266	$a = 0.54978$
	Higuchi model	$M_t/M_\infty = at^{1/2}$	0.97181	$a = 0.33407$
	Ritger-Peppas model	$M_t/M_\infty = bt^a$	0.99772	$b = 0.48948$ $a = 0.34793$
GA-CG-K ₁₀₀	Zero order model	$M_t/M_\infty = at$	0.85127	$a = 0.10104$
	First order model	$\ln(1 - M_t/M_\infty) = -at$	0.9122	$a = 0.45737$
	Higuchi model	$M_t/M_\infty = at^{1/2}$	0.98563	$a = 0.33848$
	Ritger-Peppas model	$M_t/M_\infty = bt^a$	0.99806	$b = 0.44544$ $a = 0.38869$
GA-CG-K ₂₅₀	Zero order model	$M_t/M_\infty = at$	0.63895	$a = 0.21909$
	First order model	$\ln(1 - M_t/M_\infty) = -at$	0.99139	$a = 1.75062$
	Higuchi model	$M_t/M_\infty = at^{1/2}$	0.86651	$a = 0.5385$
	Ritger-Peppas model	$M_t/M_\infty = bt^a$	0.72731	$b = 0.70243$

model

$a = 0.32091$
